

# Effect of magnetic field on spontaneous Fermi surface symmetry breaking

Hiroyuki Yamase

*Max-Planck-Institute for Solid State Research,  
Heisenbergstrasse 1, D-70569 Stuttgart, Germany*

(Dated: March 28, 2022)

## Abstract

We study magnetic field effects on spontaneous Fermi surface symmetry breaking with  $d$ -wave symmetry, the so-called  $d$ -wave “Pomeranchuk instability”. We use a mean-field model of electrons with a pure forward scattering interaction on a square lattice. When either the majority or the minority spin band is tuned close to the van Hove filling by a magnetic field, the Fermi surface symmetry breaking occurs in both bands, but with a different magnitude of the order parameter. The transition is typically of second order at high temperature and changes to first order at low temperature; the end points of the second order line are tricritical points. This qualitative picture does not change even in the limit of a large magnetic field, although the magnetic field substantially suppresses the transition temperature at the van Hove filling. The field produces neither a quantum critical point nor a quantum critical end point in our model. In the weak coupling limit, typical quantities characterizing the phase diagram have a field-independent single energy scale while its dimensionless coefficient varies with the field. The field-induced Fermi surface symmetry breaking is a promising scenario for the bilayer ruthenate  $\text{Sr}_3\text{Ru}_2\text{O}_7$ , and future issues are discussed to establish such a scenario.

PACS numbers: 71.18.+y, 75.30.Kz, 74.70.Pq, 71.10.Fd

## I. INTRODUCTION

Usually the Fermi surface (FS) respects the point-group symmetry of the underlying lattice structure. However, recently a symmetry-breaking Fermi surface deformation with a  $d$ -wave order parameter, where the FS expands along the  $k_x$  direction and shrinks along the  $k_y$  direction, or vice versa, was discussed in various two-dimensional interacting electron model on a square lattice, the  $t$ - $J$ , [1, 2, 3] Hubbard, [4, 5, 6] and extended Hubbard [7] model. This  $d$ -wave type Fermi surface deformation ( $d$ FSD) is often called  $d$ -wave Pomeranchuk instability, referring to Pomeranchuk's stability criterion for isotropic Fermi liquids. [8] However, the Fermi surface symmetry breaking can happen even without breaking such a criterion, since the instability is usually of first order at low temperature. [9, 10] Moreover, the new concept of the Fermi surface symmetry breaking is applicable also to strongly correlated electron systems such as those described by the  $t$ - $J$  model. [1, 2, 3] The  $d$ FSD instability is driven by forward scattering processes of electrons close to van Hove points in the two-dimensional Brillouin zone. The instability is thus purely electronic and the lattice does not play a role. As a result, symmetry of an electronic state is reduced from  $C_{4v}$  to  $C_{2v}$ , while the lattice retains  $C_{4v}$  symmetry as long as no electron-phonon coupling is considered.

The  $d$ FSD competes with superconductivity. Several analyses of the Hubbard [11, 12] and  $t$ - $J$  [1, 3] model showed that the  $d$ -wave superconductivity becomes a leading instability and the spontaneous  $d$ FSD does not happen. However, appreciable correlations of the  $d$ FSD remain. [13] As a result, the system becomes very sensitive to a small external  $xy$ -anisotropy and shows a giant response to it, leading to a strongly deformed FS. This idea was invoked for high-temperature cuprate superconductors. [1] In particular, the recently observed anisotropy of magnetic excitations in  $\text{YBa}_2\text{Cu}_3\text{O}_{6+x}$  [14] has been well understood in terms of  $d$ FSD correlations in the  $t$ - $J$  model. [15] Although the reduced symmetry due to the  $d$ FSD is the same as the electronic nematic phase proposed in the context of the so-called spin-charge stripes, [16] the underlying physics is very different. The Fermi surface symmetry breaking does not require the assumption of charge stripes, but is driven by forward scattering processes of electrons. The  $d$ FSD provides an essentially different route to the nematic phase.

Although a spontaneous  $d$ FSD has not been proposed for cuprates because of the competition with the  $d$ -wave singlet pairing, [1, 3] the material  $\text{Sr}_3\text{Ru}_2\text{O}_7$  turned out to have an

interesting possibility of a spontaneous  $d$ FSD.[17]  $\text{Sr}_3\text{Ru}_2\text{O}_7$  is the bilayered ruthenate with two metallic  $\text{RuO}_2$  planes where Ru-ions form a square lattice. Unlike the corresponding single-layered material  $\text{Sr}_2\text{RuO}_4$ , a well-known triplet superconductor,[18]  $\text{Sr}_3\text{Ru}_2\text{O}_7$  has a paramagnetic ground state.[19] However, the material is close to a ferromagnetic transition, which was suggested by the strongly enhanced uniform magnetic susceptibility with a large Wilson ratio,[20] uniaxial-pressure-induced ferromagnetic transition,[21] inelastic neutron scattering,[22] and band structure calculations.[23, 24] By applying a magnetic field  $h$ ,  $\text{Sr}_3\text{Ru}_2\text{O}_7$  shows a metamagnetic transition at  $h = h_c$ , around which non-Fermi liquid behavior was observed in various quantities: resistivity,[25, 26] specific heat,[26, 27, 28] thermal expansion,[29] and nuclear spin-lattice relaxation rate.[30] This non-Fermi liquid behavior was frequently discussed in terms of a putative metamagnetic quantum critical end point (QCEP), and in fact  $\text{Sr}_3\text{Ru}_2\text{O}_7$  was often referred to as a system with a metamagnetic QCEP.[31] However, after improving sample quality, the hypothetical QCEP turned out to be hidden by a dome-shaped transition line of some ordered phase around  $h_c$ .[17] While a second order transition was speculated to occur around the center of the dome, a first order transition was confirmed at the edges of the transition line and was accompanied by a metamagnetic transition. Grigera *et al.*[17] associated this instability with the spontaneous  $d$ FSD, which turned out to be consistent with a large magnetoresistive anisotropy recently observed inside the dome-shaped transition line.[32]

Any first order transition as a function of a magnetic field is generically accompanied by a metamagnetic transition, which follows from the stability of the thermodynamic potential. This was demonstrated in the case of the first order  $d$ FSD transition in connection with  $\text{Sr}_3\text{Ru}_2\text{O}_7$ .[33] Quite recently we showed that the most salient features observed in  $\text{Sr}_3\text{Ru}_2\text{O}_7$ , not only the metamagnetic transition but also the phase diagram and the non-Fermi liquid like behavior of the uniform magnetic susceptibility and the specific heat coefficient, are well captured in terms of the  $d$ FSD instability near the van Hove singularity without invoking a putative QCEP.[34] We also predicted anomalies associated with the  $d$ FSD instability in the temperature dependence of the magnetic susceptibility and the specific heat.[34]

The main purpose of this paper is to expand our previous paper about the  $d$ FSD instability in the presence of a magnetic field.[34] It is particularly interesting to perform a comprehensive analysis of magnetic field effects on the  $d$ FSD instability, since a magnetic field is often employed as a tuning parameter of a quantum phase transition. A naive ques-

tion may be whether a QCEP is realized for the  $d$ FSD instability as for the ferromagnetic instability.[35, 36] The phase diagram of the  $d$ FSD is known to be characterized by several universal numbers,[10] which can be compared directly with experimental data. It is then interesting also how the universal numbers evolve in the presence of a magnetic field.

We analyze the  $d$ FSD instability in the charge channel in a one-band model on a square lattice. The model describes electrons interacting via a pure forward scattering interaction driving the  $d$ FSD in the presence of a magnetic field (Sec. II). We solve this model numerically in Sec. III and investigate the weak coupling limit analytically in Sec. IV. In Sec. V, we discuss the reported phase diagram for  $\text{Sr}_3\text{Ru}_2\text{O}_7$ [17] as well as relations to other scenarios such as a QCEP,[31, 35, 37] phase separation,[38] and magnetic domain formation.[39] Section VI is the conclusion. In Appendix A, detailed features of the  $d$ FSD phase diagram are presented. In Appendix B, we analyze the  $d$ FSD instability in the spin channel, often called *spin-dependent Pomeranchuk instability*, which shows exactly the same phase diagram as in the charge channel.

## II. MODEL AND FORMALISM

We investigate the  $d$ FSD instability in the charge channel under a magnetic field on a square lattice. The minimal model reads

$$H = \sum_{\mathbf{k},\sigma} (\epsilon_{\mathbf{k}}^0 - \mu) n_{\mathbf{k}\sigma} + \frac{1}{2N} \sum_{\mathbf{k},\sigma,\mathbf{k}',\sigma'} f_{\mathbf{k}\mathbf{k}'} n_{\mathbf{k}\sigma} n_{\mathbf{k}'\sigma'} - h \sum_{\mathbf{k},\sigma} \sigma n_{\mathbf{k}\sigma} \quad (1)$$

where  $n_{\mathbf{k}\sigma} = c_{\mathbf{k}\sigma}^\dagger c_{\mathbf{k}\sigma}$  counts the electron number with momentum  $\mathbf{k}$  and spin  $\sigma$ ;  $c_{\mathbf{k}\sigma}^\dagger$  ( $c_{\mathbf{k}\sigma}$ ) is an electron creation (annihilation) operator;  $\mu$  is the chemical potential;  $N$  is the number of lattice sites;  $h$  is an effective magnetic field and is defined as  $h = \frac{1}{2}\mathbf{g}\mu_B H$  where  $\mathbf{g}$  is a  $g$ -factor,  $\mu_B$  is Bohr magneton, and  $H$  is a magnetic field. For hopping amplitudes  $t$  and  $t'$  between nearest and next-nearest neighbors on the square lattice, respectively, the bare dispersion relation is given by

$$\epsilon_{\mathbf{k}}^0 = -2t(\cos k_x + \cos k_y) - 4t' \cos k_x \cos k_y. \quad (2)$$

The forward scattering interaction driving the spontaneous  $d$ FSD has the form

$$f_{\mathbf{k}\mathbf{k}'} = -g d_{\mathbf{k}} d_{\mathbf{k}'}, \quad (3)$$

with a coupling constant  $g \geq 0$  and a  $d$ -wave form factor  $d_{\mathbf{k}} = \cos k_x - \cos k_y$ . This ansatz mimics the structure of the effective interaction in the forward scattering channel as obtained for the  $t$ - $J$ ,[1] Hubbard,[4] and extended Hubbard[7] model. For  $h = 0$ , this model and a similar model were studied in Refs. 10 and 9, respectively.

We decouple the interaction by introducing a spin-dependent mean field

$$\eta_{\sigma} = -\frac{g}{N} \sum_{\mathbf{k}} d_{\mathbf{k}} \langle n_{\mathbf{k}\sigma} \rangle, \quad (4)$$

which becomes finite when the system breaks orientational symmetry and is thus the order parameter of the  $d$ FSD. The mean-field Hamiltonian reads

$$H_{\text{MF}} = \sum_{\mathbf{k}, \sigma} \xi_{\mathbf{k}\sigma} n_{\mathbf{k}\sigma} + \frac{N}{2g} \eta^2, \quad (5)$$

where

$$\xi_{\mathbf{k}\sigma} = \epsilon_{\mathbf{k}}^0 + \eta d_{\mathbf{k}} - \mu_{\sigma}. \quad (6)$$

Here the  $\sigma$ -summed mean field  $\eta = \sum_{\sigma} \eta_{\sigma}$  enters  $\xi_{\mathbf{k}\sigma}$ , and thus a finite  $\eta_{\sigma}$  in general induces a finite  $\eta_{-\sigma}$ ; the magnetic field is absorbed completely in the effective chemical potential  $\mu_{\sigma} = \mu + \sigma h$ . The grand canonical potential per lattice site is given by

$$\omega = -\frac{T}{N} \sum_{\mathbf{k}\sigma} \log(1 + e^{-\xi_{\mathbf{k}\sigma}/T}) + \frac{\eta^2}{2g}. \quad (7)$$

By minimizing Eq. (7) with respect to  $\eta$ , we obtain a self-consistency equation

$$\eta = -\frac{g}{N} \sum_{\mathbf{k}, \sigma} d_{\mathbf{k}} f(\xi_{\mathbf{k}\sigma}). \quad (8)$$

We consider the solution with  $\eta \geq 0$ , since the free energy Eq. (7) is an even function with respect to  $\eta$ . The self-consistency equation is written also as

$$\eta_{\sigma} = -\frac{g}{N} \sum_{\mathbf{k}} d_{\mathbf{k}} f(\xi_{\mathbf{k}\sigma}). \quad (9)$$

Note that our Hamiltonian (1) does not allow momentum transfer, and thus the mean-field theory solves our model exactly in the thermodynamic limit.

### III. NUMERICAL RESULTS

LDA band calculations[23, 24] for  $\text{Sr}_3\text{Ru}_2\text{O}_7$  without a magnetic field showed that the electronic structure is similar to that for the single-layered material  $\text{Sr}_2\text{RuO}_4$  except that

there are six FSs because of the bilayered structure. Since the  $d$ FSD instability is driven by electrons near the van Hove points on a square lattice, we focus on the FS closest to  $\mathbf{k} = (\pi, 0)$  and  $(0, \pi)$ , and mimic such a FS by choosing  $t'/t = 0.35$ . For  $h = 0$  the bare dispersion has the van Hove energy at  $4t' = 1.4t$ , from which we measure the chemical potential  $\mu$ . We take  $g/t = 1$  for numerical convenience, but the result for  $g/t = 0.5$  shall be mentioned in the context of Fig. 4. We set  $t = 1$  so that all quantities with dimension of energy are in units of  $t$ , and consider a region of  $h \geq 0$  in this paper since the result is symmetric with respect to  $h \rightarrow -h$  and  $\sigma \rightarrow -\sigma$ .

Figure 1(a) shows a phase diagram for  $\mu = -0.4$  in the plane of the magnetic field  $h$  and temperature  $T$ ; the dotted line at  $h = h_{\text{vH}} = 0.4$  represents the van Hove energy of the up-spin band (majority band). The  $d$ FSD transition is of second order for high  $T$  and changes to first order for low  $T$ ; the end points of the second order line are tricritical points. Hence the transition line forms a domed shape around the van Hove energy. Figure 1(b) shows the  $h$  dependence of the order parameter  $\eta$  for low  $T$  together with  $\eta_{\uparrow}$  and  $\eta_{\downarrow}$ . We see that although the phase transition happens around the van Hove energy of the up-spin band, both  $\eta_{\uparrow}$  and  $\eta_{\downarrow}$  show a jump at the first order point; the  $\eta_{\uparrow}$  has the same sign as  $\eta_{\downarrow}$ , but with a different magnitude. The FSs at  $T = 0.01$  are shown in Fig. 1(c) and (d) for  $h = 0.3$  and  $0.5$ , respectively, together with the FSs for  $g = 0$ ; the outer (inner) FS corresponds to the up-spin (down-spin) electron band; the splitting of the FSs is due to the Zeeman energy. The FS instability drives a deformation of both FSs and typically leads to an open outer FS. Electron density for each spin also shows a jump at the first order transition point, but the size of the jump is different [Fig. 1(e)]. This difference yields a metamagnetic transition as shown in Fig. 1(f). This is a generic consequence of the concavity of the grand canonical potential when a first order transition occurs as a function of  $h$ , the canonical conjugate quantity to the magnetization  $m$ . The metamagnetic transition disappears for high  $T$  where the  $d$ FSD transition becomes second order. The  $T$  dependence of the magnetization is shown in Fig. 1(g) for several choices of  $h$ . The magnetization shows a kink at the second order transition. Roughly speaking, compared with the non-interacting case, the magnetization is enhanced (suppressed) by the  $d$ FSD transition for  $h \lesssim h_{\text{vH}}$  ( $h \gtrsim h_{\text{vH}}$ ). Since the transition is of first order for low  $T$  as a function of  $h$ , there appears a phase separation as a function of the magnetization [Fig. 1(h)]. The width of the phase separated region corresponds to a magnitude of a jump of  $m$  at the first order transition point seen in Fig. 1(f).

The  $d$ FSD instability has a dome-shaped transition line around the van Hove energy of the up-spin band for the chemical potential ( $\mu < 0$ ) as shown in Fig. 1(a). When one invokes much larger  $\mu (> 0)$ , the  $d$ FSD transition then happens around the van Hove energy of the down-spin band. When  $\mu$  is around zero, the second order line extends down to  $h = 0$  and a first order line appears only on the larger  $h$  side for low  $T$  as shown in Fig. 2. For some special values of  $\mu$ , see Appendix A.

Although a metamagnetic transition generically accompanies a first order  $d$ FSD phase transition, the metamagnetic transition can also occur inside the symmetry-broken phase because of a level crossing between two local minima of the free energy. This is actually the case in the present model as demonstrated in Fig. 3, where  $m$  is plotted as a function of  $h$  for  $\mu = -0.2$ ; the  $h$  dependence of the order parameter is shown in the inset. In addition to a jump associated with the first order  $d$ FSD transition at  $h \approx 0.34$  (see also Fig. 2), another metamagnetic transition appears at  $h \approx 0.28$  in the symmetry-broken phase. This metamagnetic transition is a weak feature in the sense that it is smeared out by thermal broadening for a relatively low temperature while the metamagnetic transition associated with the  $d$ FSD instability from the symmetric state is robust up to  $T = T_c^{\text{tri}}$ .

Figure 4(a) summarizes numerical results in the plane of  $(\mu, h)$  at low  $T = 0.01$ ; the solid circles denote a first order transition to the symmetry-broken phase, where the order parameter  $\eta$  shows a jump from zero to a finite value, accompanied by a metamagnetic transition as a function of  $h$ ; the cross symbols are positions, where a first order transition occurs in the symmetry-broken phase due to a level crossing of local minima of the free energy, yielding an additional metamagnetic transition; the dotted line represents positions of the van Hove energy for the up-spin band ( $\mu < 0$ ) and the down-spin band ( $\mu > 0$ ). We see that the  $d$ FSD phase is stabilized around the van Hove energy of each spin band as a function of  $h$  for a given  $\mu$ . With respect to the axis  $\mu = 0$ , the phase diagram is nearly symmetric and becomes fully symmetric when  $t'$  is set to be zero. When we take a smaller  $g$ , the symmetry-broken phase is stabilized closer to the van Hove energy, but the qualitative features of Fig. 4(a) do not change except that the energy scale is substantially decreased.

We define  $T_c^{\text{vH}}$  as  $T_c$  at the van Hove energy, namely at  $h = |\mu|$ , and show its  $h$  dependence in Figs. 4(b) and (c) for  $\mu < 0$  and  $\mu > 0$ , respectively. The  $T_c^{\text{vH}}$  is suppressed with increasing magnetic field. In particular, for a smaller  $g$ , a relatively small  $h$  suppresses  $T_c^{\text{vH}}$  drastically. However, the suppression saturates for larger  $h$ , leading to a finite  $T_c^{\text{vH}}$ , where we obtain a

phase diagram similar to Fig. 1(a). That is, neither a quantum critical point (QCP) nor a QCEP of the  $d$ FSD is realized by the magnetic field, which we will further discuss in Sec. IV.

#### IV. WEAK COUPLING LIMIT

The  $d$ FSD instability occurs around the van Hove filling and thus the transition is dominated by states with momentum near the saddle points of  $\epsilon_{\mathbf{k}}^0$ . In the weak coupling limit, therefore, the mean-field equations can be treated analytically by focusing on the state near the saddle points, similar to the analysis in Ref.10 in the absence of a magnetic field. Since the magnetic field is absorbed completely in the effective chemical potential  $\mu_\sigma = \mu + \sigma h$ , we can extend such an analysis to the present case by allowing the  $\sigma$  dependence of the chemical potential. The chemical potential  $\mu$  is measured from the van Hove energy at  $h = 0$  so that  $\mu_\sigma = 0$  indicates that the  $\sigma$ -spin band is at the van Hove filling. We first determine a zero temperature phase diagram in the plane of  $(\mu, h)$ , and then investigate  $T_c$  suppression by a magnetic field,  $\mu$  dependence of typical quantities characterizing the phase diagram, and the limit  $h \rightarrow \infty$ .

##### A. Zero temperature phase diagram

Following the analysis in Ref.10, the self-consistency equation Eq. (8) is written as

$$\eta = \frac{\bar{g}}{2} \sum_{\sigma} [(\mu_{\sigma} - \eta) \log |\mu_{\sigma} - \eta| - (\mu_{\sigma} + \eta) \log |\mu_{\sigma} + \eta| + 2\eta (1 + \log \epsilon_{\Lambda})], \quad (10)$$

where  $\bar{g} = 2mg/\pi^2$  is the dimensionless coupling and  $\epsilon_{\Lambda} = \Lambda^2/(2m)$  is a cutoff energy;  $m$  is the effective mass near the van Hove energy and is related to the hopping integrals  $t$  and  $t'$ .

The grand canonical potential is then given by

$$\begin{aligned} \omega(\eta; \mu, h) = & \frac{2m}{\pi^2} \left\{ \left[ \frac{1}{2\bar{g}} - \frac{1}{2} - (1 + \log \epsilon_{\Lambda}) \right] \eta^2 \right. \\ & \left. + \frac{1}{2} \sum_{\sigma} \left[ \frac{1}{2} (\mu_{\sigma} + \eta)^2 \log |\mu_{\sigma} + \eta| + \frac{1}{2} (\mu_{\sigma} - \eta)^2 \log |\mu_{\sigma} - \eta| \right] \right\} + \text{const.} \quad (11) \end{aligned}$$

It is not difficult to see that Eqs. (10) and (11) are symmetric with respect to interchange of  $h$  and  $\mu$ , that is, the magnetic field  $h$  plays exactly the same role as the chemical potential  $\mu$ .

We focus on the region  $0 \leq \mu < h$  and introduce rescaled variables  $\tilde{\eta} = \eta/h$  and  $\tilde{\mu}_{\sigma} = \tilde{\mu} + \sigma$



with  $\tilde{\mu} = \mu/h$ . Equation (10) then reads

$$\frac{\tilde{\eta}}{\tilde{g}} = \frac{1}{2} \sum_{\sigma} [(\tilde{\mu}_{\sigma} - \tilde{\eta}) \log |\tilde{\mu}_{\sigma} - \tilde{\eta}| - (\tilde{\mu}_{\sigma} + \tilde{\eta}) \log |\tilde{\mu}_{\sigma} + \tilde{\eta}|] \quad (12)$$

with a renormalized coupling constant

$$\tilde{g}^{-1} = \bar{g}^{-1} + 2 \log h - 2(1 + \log \epsilon_{\Lambda}) . \quad (13)$$

Similarly Eq. (11) is written as  $\omega(\eta; \mu, h) = \frac{2m}{\pi^2} h^2 \tilde{\omega}(\tilde{\eta}; \tilde{\mu})$ , where

$$\begin{aligned} \tilde{\omega}(\tilde{\eta}; \tilde{\mu}) = & \left( \frac{1}{2\tilde{g}} - \frac{1}{2} \right) \tilde{\eta}^2 - \frac{1}{2} \sum_{\sigma} \tilde{\mu}_{\sigma}^2 \log |\tilde{\mu}_{\sigma}| \\ & + \frac{1}{2} \sum_{\sigma} \left[ \frac{1}{2} (\tilde{\mu}_{\sigma} + \tilde{\eta})^2 \log |\tilde{\mu}_{\sigma} + \tilde{\eta}| + \frac{1}{2} (\tilde{\mu}_{\sigma} - \tilde{\eta})^2 \log |\tilde{\mu}_{\sigma} - \tilde{\eta}| \right] \end{aligned} \quad (14)$$

and the energy is shifted such that  $\tilde{\omega}(\tilde{\eta} = 0; \tilde{\mu}) = 0$ .

At zero temperature, the  $d$ FSD transition is usually of first order as we have seen in Figs. 1(a) and 2. The first order transition is determined by solving Eq. (12) and  $\tilde{\omega}(\tilde{\eta}; \tilde{\mu}) = 0$  numerically for a given  $\tilde{\mu}$ , yielding a solution  $\tilde{\eta}_1$  and  $\tilde{g}_1$ . A corresponding magnetic field  $h_1$  is then obtained from Eq. (13)

$$h_1 = \exp \left( 1 + \frac{1}{2\tilde{g}_1(\tilde{\mu})} \right) \epsilon_{\Lambda} e^{-1/(2\tilde{g})} , \quad (15)$$

and thus the chemical potential and the order parameter are  $|\mu_1| = \tilde{\mu} h_1$  and  $\eta_1 = \tilde{\eta}_1 h_1$ , respectively. All quantities,  $h_1$ ,  $\mu_1$ , and  $\eta_1$ , are determined by a single energy scale  $\epsilon_{\Lambda} e^{-1/(2\tilde{g})}$  and the magnetic field just changes its dimensionless coefficient. We plot  $(\mu_1, h_1)$  in Fig. 5; the phase diagram is symmetric with respect to the  $\mu = 0$  axis and the  $h = |\mu|$  axis; such symmetry is not seen in our numerical result [Fig. 4(a)], since a finite  $t'$  breaks the symmetry when  $g$  is not in the weak coupling limit. The first order transition line has a kink at  $|\mu| \approx 1.3\epsilon_{\Lambda} e^{-1/(2\tilde{g})}$  and  $h \approx 0.54\epsilon_{\Lambda} e^{-1/(2\tilde{g})}$  (see the inset of Fig. 5). At this point, the solution of  $\tilde{\omega}(\tilde{\eta}; \tilde{\mu}) = 0$  [Eq. (14)] shows a jump, indicating double local minima of the free energy  $\tilde{\omega}(\tilde{\eta})$  away from  $\tilde{\eta} = 0$ , which then may yield an additional first order transition in the symmetry-broken phase as seen in Figs. 3 and 4(a).

## B. $T_c$ suppression by a magnetic field

A magnetic field suppresses the  $d$ FSD transition temperature [Fig. 4(b)]. Here we clarify key factors of this suppression.

Since the  $d$ FSD transition is of second order as a function of  $T$  at the van Hove filling, the  $T_c$  is obtained by linearizing the right-hand side of Eq. (8) with respect to  $\eta$ , namely

$$1 = gN_2(\mu, h, T_c), \quad (16)$$

where we introduce

$$N_p(\mu, h, T) = -\frac{1}{N} \sum_{\mathbf{k}, \sigma} d_{\mathbf{k}}^p f'(\epsilon_{\mathbf{k}}^0 - \mu_\sigma), \quad (17)$$

a weighted density of states averaged over an energy interval of order  $T$  around  $\mu_\sigma$ ;  $p$  is an even integer;  $f'$  is a first derivative of Fermi distribution function with respect to  $\epsilon_{\mathbf{k}}^0$ . In the weak coupling limit[10], Eq. (17) reads

$$N_p(\mu, h, T) = -\frac{2m}{\pi^2} \sum_{\sigma} \int_{-\epsilon_\Lambda}^{\epsilon_\Lambda} d\epsilon \log \frac{\epsilon_\Lambda}{|\epsilon|} f'(\epsilon - \mu_\sigma). \quad (18)$$

No  $p$  dependence appears on the right-hand side, since we have redefined  $d_{\mathbf{k}} = \frac{1}{2}(\cos k_x - \cos k_y)$  in the present analysis in the weak coupling limit[10] so that  $|d_{\mathbf{k}}| = 1$  at  $\mathbf{k} = (\pi, 0)$  and  $(0, \pi)$ , namely at the saddle points of  $\epsilon_{\mathbf{k}}^0$ . The van Hove filling of the  $\sigma$  spin electron band is set by choosing

$$\mu_\sigma = \mu + \sigma h = 0, \quad \mu_{-\sigma} = \mu - \sigma h = -2\sigma h. \quad (19)$$

We consider the  $\sigma = \downarrow$  case, namely for  $\mu > 0$  and  $h > 0$ . Since

$$-\int_{-\epsilon_\Lambda}^{\epsilon_\Lambda} d\epsilon \log \frac{\epsilon_\Lambda}{|\epsilon|} f'(\epsilon - 2h) \xrightarrow{\epsilon_\Lambda/T \rightarrow \infty} \log \epsilon_\Lambda + a(h, T), \quad (20)$$

where

$$a(h, T) = \int_{-\infty}^{\infty} dx \log |Tx + 2h| \frac{\partial}{\partial x} \frac{1}{e^x + 1}, \quad (21)$$

we obtain

$$N_2(h, T) = \frac{2m}{\pi^2} \left[ 2 \log \frac{2\epsilon_\Lambda e^\gamma}{\pi T} + a(h, T) - a(0, T) \right]. \quad (22)$$

where  $a(0, T) = \log[2e^\gamma/(\pi T)]$  with Euler constant  $\gamma \approx 0.577$ . Defining a rescaled variable  $\tilde{h}_T = h/T$ , we may write

$$\begin{aligned} \zeta(\tilde{h}_T) &= a(0, T) - a(h, T) \\ &= \log \frac{2e^\gamma}{\pi} - \int_{-\infty}^{\infty} dx \log |x + 2\tilde{h}_T| \frac{\partial}{\partial x} \frac{1}{e^x + 1}, \end{aligned} \quad (23)$$

where  $\zeta(\tilde{h}_T)$  increases monotonically with  $\tilde{h}_T$ , and  $\zeta(0) = 0$  and  $\zeta(\tilde{h}_T) = \zeta(-\tilde{h}_T)$ . Substituting Eq. (22) into Eq. (16), we obtain  $T_c^{\text{vH}}$  at the van Hove filling for a given  $\tilde{h}_T$

$$T_c^{\text{vH}} = \frac{2e^\gamma}{\pi} \epsilon_\Lambda e^{-1/(2\bar{g})} e^{-\frac{1}{2}\zeta(\tilde{h}_T)} \quad (24)$$

$$= T_c^{\text{vH}}(0) e^{-\frac{1}{2}\zeta(\tilde{h}_T)} \quad (25)$$

where

$$T_c^{\text{vH}}(0) = \frac{2e^\gamma}{\pi} \epsilon_\Lambda e^{-1/(2\bar{g})} \quad (26)$$

is the critical temperature for  $h = 0$ ; the corresponding magnetic field is obtained as  $h = \tilde{h}_T T_c^{\text{vH}}$ . We evaluate  $\zeta(\tilde{h}_T)$  numerically and show in Fig. 6 the  $h$  dependence of  $T_c^{\text{vH}}$ . The  $T_c^{\text{vH}}$  is suppressed with  $h$ , as we have seen in Fig. 4(b). Defining a magnetic field  $h_{1/2}$ , at which  $T_c^{\text{vH}}$  is suppressed down to a half value of  $T_c^{\text{vH}}(0)$ , we read off  $h_{1/2} = 1.00 T_c^{\text{vH}}(0)$  from Fig. 6. Therefore from Eq. (26) we obtain

$$h_{1/2} \propto \epsilon_\Lambda e^{-1/(2\bar{g})}, \quad (27)$$

that is, the suppression of  $T_c^{\text{vH}}$  is controlled by the dimensionless coupling constant  $\bar{g} = 2mg/\pi^2$ . When  $g$  becomes smaller,  $h_{1/2}$  gets smaller exponentially, leading to a strong suppression of  $T_c^{\text{vH}}$  by the magnetic field. Similarly, the smaller effective mass suppresses  $T_c$  substantially with a magnetic field.

### C. $\mu$ dependence of characteristic quantities of the phase diagram

We have derived the analytic expressions for  $h_1$  [Eq. (15)] and  $T_c^{\text{vH}}$  [Eq. (24)]. There is another important quantity characterizing the  $d\text{FSD}$  phase diagram, the tricritical point  $(T_c^{\text{tri}}, h_{\text{tri}})$ , which we first calculate for a given  $\mu$ . We then summarize how  $h_1$ ,  $T_c^{\text{vH}}$ ,  $T_c^{\text{tri}}$ , and  $h_{\text{tri}}$  evolve as a function of  $\mu$ . Since all these quantities are scaled by a single energy, ratios of these different quantities become universal, whose  $\mu$  dependence is also clarified.

At the tricritical point, both the quadratic and quartic coefficient of the Landau free energy,  $\omega(\eta)$ , vanish simultaneously. This condition is determined by Eq. (16) and

$$\frac{\partial^2}{\partial \mu^2} N_4(\mu, h, T) = 0 \quad (28)$$

where  $N_4$  is defined in Eq. (17). While we have analyzed Eq. (16) at the van Hove point [Eq. (19)] in the previous section, we here consider Eq. (16) for general  $\mu_\sigma$  and obtain

$$T_c^{\text{tri}} = e^\alpha \epsilon_\Lambda e^{-1/(2\bar{g})}, \quad (29)$$

where

$$\alpha(\tilde{\mu}_T, \tilde{h}_T) = \frac{1}{2} \sum_{\sigma} \int_{-\infty}^{\infty} dx \log |x + \tilde{\mu}_T + \sigma \tilde{h}_T| \frac{\partial}{\partial x} \frac{1}{e^x + 1} \quad (30)$$

with  $\tilde{\mu}_T = \mu/T$ . Similarly Eq. (28) is written in the weak coupling limit as

$$\frac{1}{2} \sum_{\sigma} \int_{-\infty}^{\infty} dx \log |x + \tilde{\mu}_T + \sigma \tilde{h}_T| \frac{\partial^3}{\partial x^3} \frac{1}{e^x + 1} = 0. \quad (31)$$

It is easy to observe that Eqs. (30) and (31) are symmetric with respect to  $\tilde{\mu}_T \leftrightarrow \tilde{h}_T$  and thus  $h$  plays exactly the same role as  $\mu$ . We solve Eq. (31) numerically for a given  $\tilde{\mu}_T$  and determine  $\tilde{h}_T$ . The tricritical temperature  $T_c^{\text{tri}}$  is then obtained from Eqs. (29) and (30); the original  $\mu$  and  $h$  are determined as  $h_{\text{tri}} = \tilde{h}_T T_c^{\text{tri}}$  for a given  $\mu = \tilde{\mu}_T T_c^{\text{tri}}$ . Figure 7(a) summarizes  $T_c^{\text{vH}}$ ,  $T_c^{\text{tri}}$ ,  $h_{\text{tri}}$ , and  $h_1$  as a function of  $\mu$ . We see that all quantities are suppressed with increasing  $|\mu|$ , but do not reach zero; in fact they approach certain asymptotic values as we show in the next subsection. Since all quantities are scaled by the single energy, we obtain universal numbers by taking ratios of the different quantities. In Fig. 7(b), we plot representative universal ratios  $T_c^{\text{tri}}/T_c^{\text{vH}}$  and  $T_c^{\text{tri}}/|h_{\text{tri}} - h_{\text{vH}}|$ , where  $h_{\text{vH}}$  is the van Hove energy and is given by  $h_{\text{vH}} = |\mu|$ . The strong  $\mu$  dependence appears for relatively small  $\mu$  and the variation is within a factor of 1.5.

Although universal ratios are obtained in the weak coupling limit, these numbers also characterize well the phase diagram for a relatively large  $g$ . For example in Fig. 1(a),  $T_c^{\text{tri}}/|h_{\text{tri}} - h_{\text{vH}}| \approx 0.5 - 0.6$  and  $T_c^{\text{tri}}/T_c^{\text{vH}} \approx 0.5 - 0.75$ , which are comparable values to those in Fig. 7(b).

#### D. Large $h$ limit

For a larger  $\mu$ , each quantity in Fig. 7(a) approaches a certain asymptotic value. In addition, the universal ratios in Fig. 7(b) converge to the same values as those at  $\mu = 0$ . To understand such asymptotic behavior, we consider  $T_c^{\text{vH}}$  in the limit  $\mu_{\uparrow} \rightarrow \infty$  while keeping  $\mu_{\downarrow} = 0$  [see Eq. (19)], namely, the limit of  $\mu \rightarrow \infty$  and  $h \rightarrow \infty$ . Since the up-spin electron band becomes fully occupied, we have  $f'(\epsilon - \mu_{\uparrow}) = 0$  for  $|\epsilon| < \epsilon_{\Lambda}$ . Hence from Eq. (18) we have

$$N_2(T) = -\frac{2m}{\pi^2} \int_{-\epsilon_{\Lambda}}^{\epsilon_{\Lambda}} d\epsilon \log \frac{\epsilon_{\Lambda}}{|\epsilon|} f'(\epsilon) \quad (32)$$

$$\xrightarrow{\epsilon_{\Lambda}/T \rightarrow \infty} \frac{2m}{\pi^2} \log \frac{2\epsilon_{\Lambda} e^{\gamma}}{\pi T}. \quad (33)$$

The gap equation Eq. (16) then yields

$$T_c^{\text{vH}} = \frac{2e^\gamma}{\pi} \epsilon_\Lambda e^{-1/\bar{g}} \quad (34)$$

$$= T_c^{\text{vH}}(0) e^{-1/(2\bar{g})}. \quad (35)$$

That is, the  $d\text{FSD}$  transition occurs even for  $h \rightarrow \infty$  under the condition of  $h = |\mu|$ , although  $T_c^{\text{vH}}$  is suppressed a factor of  $e^{-1/(2\bar{g})}$  compared to the case of  $h = 0$ . Since the other spin band is fully occupied (empty) for  $\mu \rightarrow +\infty$  ( $\mu \rightarrow -\infty$ ), only one spin band is subject to the  $d\text{FSD}$  instability. Therefore in the  $h \rightarrow \infty$  limit, our model is reduced to a “spinless” fermion model, and thus the same results as those for  $h = 0$  (Sec. V in Ref. 10) are obtained except that the energy scale is replaced by  $\epsilon_\Lambda e^{-1/\bar{g}}$ . Hence various ratios of different quantities characterizing the phase diagram show exactly the same universal numbers as those for  $h = 0$ . The magnetic field just reduces the energy scale and cannot produce a QCP nor a QCEP of the  $d\text{FSD}$  instability.

## V. RELEVANCE TO $\text{Sr}_3\text{Ru}_2\text{O}_7$

We have shown that when either the up- or the down-spin electron band is tuned by a magnetic field close to the van Hove filling, the  $d\text{FSD}$  transition occurs in both bands but with a different magnitude of the order parameter. The field-induced  $d\text{FSD}$  instability is a promising scenario for  $\text{Sr}_3\text{Ru}_2\text{O}_7$ . In fact, several important features observed experimentally such as the phase diagram, the metamagnetic transition, and the non-Fermi liquid like behavior of the magnetic susceptibility and the specific heat coefficient are well captured in terms of the  $d\text{FSD}$  instability around the van Hove filling as we have shown in Ref. 34.

On the basis of the present results, we discuss in more detail the reported phase diagram for  $\text{Sr}_3\text{Ru}_2\text{O}_7$ . [17] Since no experimental evidence of a symmetry-broken phase was obtained at  $h = 0$  and LDA band calculations [23, 24] showed that the van Hove energy is located above the Fermi energy, corresponding to  $\mu < 0$ , we expect that the chemical potential  $\mu$  is away from the van Hove energy, but rather close to it, for example  $\mu \approx -0.4$  for the parameters shown in Fig. 4. Figure 1(a) is a representative phase diagram of the magnetic field-induced  $d\text{FSD}$  instability, which is very similar to the reported phase diagram. [17] The maximal  $T_c$  in the experiment is about 1 K, which is much smaller than the energy scale in Fig. 1(a). The coupling constant  $g$  in  $\text{Sr}_3\text{Ru}_2\text{O}_7$  is thus expected to be very small. In the weak

coupling limit (Sec. IV), the phase diagram is characterized by a single energy scale  $\epsilon_{\Lambda} e^{-1/2\bar{g}}$  and thus various ratios among  $T_c^{\text{vH}}$ ,  $T_c^{\text{tri}}$ ,  $h_{\text{tri}}$ , and  $h_1$  become universal numbers [Fig. 7(b)]. The universal ratios are compared directly with experimental data. The data by Grigera *et al.*[17] provide  $T_c^{\text{vH}} \approx 1$  K,  $T_c^{\text{tri}} \sim 0.6$  K,  $h_{\text{tri}} \approx h_1 = \frac{1}{2}\mathbf{g}\mu_B H$  with  $H \approx 7.8$  and 8.1 Tesla, and  $h_{\text{vH}} = \frac{1}{2}\mathbf{g}\mu_B H_{\text{vH}}$  with  $H_{\text{vH}} \approx 7.95$  Tesla. We thus obtain  $h_{\text{tri}}/h_1 \approx 1$ ,  $T_c^{\text{tri}}/T_c^{\text{vH}} \sim 0.6$ , and  $T_c^{\text{tri}}/|h_{\text{tri}} - h_{\text{vH}}| \sim (k_B \cdot 0.6)/(\frac{1}{2}\mathbf{g}\mu_B \cdot 0.15) \approx 12\mathbf{g}^{-1}$  with Boltzmann constant  $k_B$ . The first one is consistent with our result Fig. 7(a); the value of the second one is comparable with Fig. 7(b); as for the last one, however, the discrepancy is by a factor of 10 if we assume  $\mathbf{g} = 2$ .

While the field-induced  $d\text{FSD}$  instability is well analyzed in the present model, further studies are necessary to make more quantitative comparison with experiments. (i) The interaction in our model retains  $\text{SU}(2)$  symmetry and thus the present theory cannot address the issue why the possibility of the  $d\text{FSD}$  instability was clearly observed only over a narrow region of applied field angle to the  $\text{RuO}_2$  plane.[40] One possible origin of such a field angle dependence lies in a magnetic anisotropy, which we expect to originate mainly from a relatively strong spin-orbit coupling connected with the heavy Ru-ion. Our model should be extended by taking the magnetic anisotropy into account for a more quantitative study. (ii) Inclusion of a magnetic interaction in our model may also be necessary, since  $\text{Sr}_3\text{Ru}_2\text{O}_7$  is expected to be close to a ferromagnetic transition.[20, 21, 22, 23, 24] This is suggested also by comparing Fig. 1(g) with the experimental data.[17] In Fig. 1(g) the  $d\text{FSD}$  instability produces a kink in the  $T$  dependence of  $m$  at the transition temperature  $T_c$ . This kink is actually observed in the experiment[17] and our result for  $h \gtrsim 0.35$  is similar to the experiment. But the present theory cannot reproduce the observed upward curvature of the  $T$  dependence of  $m$  for  $T > T_c$ ,[17] which may come from a magnetic interaction. (iii)  $\text{Sr}_3\text{Ru}_2\text{O}_7$  is a bilayered material. Since the  $d\text{FSD}$  instability is driven by forward scattering processes of quasi-particles near  $\mathbf{k} = (\pi, 0)$  and  $(0, \pi)$ , a form of bilayer coupling can be important if the bilayer coupling gives rise to  $k_z$  dispersion around  $\mathbf{k} = (\pi, 0)$  and  $(0, \pi)$ . Insights into the  $k_z$  dispersion will be obtained from further detailed LDA calculations.[23, 24]

The  $d\text{FSD}$  instability was discussed in basic lattice models such as two-dimensional  $t$ - $J$ ,[1, 2, 3] Hubbard,[4, 5, 6] and extended Hubbard[7] model, and can be a generic tendency near van Hove filling in correlated electron systems.[41] Hence the  $d\text{FSD}$  is an interesting

possibility when the Fermi energy is tuned close to the van Hove energy in other materials also such as  $\text{Sr}_{2-y}\text{La}_y\text{RuO}_4$ [42] where La-substitution introduces electron carriers and makes the FS closer to the van Hove point. However, La introduces some disorder in the  $\text{RuO}_2$  plane; its effects should be considered carefully, since the physics near the van Hove singularity may in general depend strongly on sample purity. In fact, the specific heat coefficient for low  $T$  in  $\text{Sr}_{2-y}\text{La}_y\text{RuO}_4$ [42] shows different behavior from that in  $\text{Sr}_3\text{Ru}_2\text{O}_7$  although both systems are expected to be nicely tuned close to the van Hove filling. It is interesting to investigate impurity effects on the  $d$ FSD instability by chemical (electron) doping to  $\text{Sr}_3\text{Ru}_2\text{O}_7$ . According to our phase diagram [Figs. 4(a) and 5, see also Appendix A], the  $d$ FSD instability can occur for a smaller magnetic field and even without the field if the impurity effect by the electron doping is not serious.

Around the van Hove filling, various ordering tendencies such as antiferromagnetism, ferromagnetism, superconductivity, and  $d$ -density wave develop,[11, 12] and compete with the  $d$ FSD instability. Since the  $d$ FSD instability is suppressed by a magnetic field and its suppression is controlled by  $\bar{g} \propto mg$  [see Eq. (27)], the absolute values of the effective mass and the coupling constant are crucial to the possible  $d$ FSD instability over other instabilities. In this sense, microscopic derivation of  $m$  and  $g$  as well as magnetic field dependences of other instabilities are important future issues.

Some order competing with the  $d$ FSD instability is in fact expected in  $\text{Sr}_3\text{Ru}_2\text{O}_7$ . While the experimental phase diagram[17] is very similar to our result Fig. 1(a), the closer comparison between them reveals a difference of slope of the first-order-transition line. In the experiment, the edges of the first order line are shifted to the center of the phase diagram so that the  $d$ FSD state is stabilized in a narrower region for lower  $T$ . This can be interpreted as development of some ordering tendency for lower  $T$  in  $\text{Sr}_3\text{Ru}_2\text{O}_7$ , which then suppresses the  $d$ FSD instability. Although a different interpretation was given in Ref. 17, a theoretical result consistent with this interpretation was indeed obtained in the case of competition of the  $d$ FSD and superconductivity.[43]

It should be kept in mind that even if the  $d$ FSD instability does not become a leading instability, the system can still keep appreciable correlations of the  $d$ FSD.[13] As a result, small external perturbations such as an anisotropic strain and a lattice anisotropy can drive sizable  $d$ -wave type FS deformations. This idea was proposed for high-temperature cuprate superconductors.[1]

$\text{Sr}_3\text{Ru}_2\text{O}_7$  is frequently referred to as a material with a metamagnetic QCEP.[31] The compelling evidence for this was the systematic decrease of a metamagnetic critical end point by rotating the magnetic field out of the plane.[44] In fact, several theoretical scenarios based on a metamagnetic QCEP were proposed.[35, 37] However, recent data for ultrapure crystals showed that the critical end point does not reach zero.[40] Quite recently we have found that several important features are already well captured even without the putative QCEP.[34] The non-Fermi liquid like behavior of the magnetic susceptibility[20] and specific heat[26, 27, 28] observed in  $\text{Sr}_3\text{Ru}_2\text{O}_7$  can originate from the van Hove singularity of the density of states. Moreover, while the first  $d\text{FSD}$  transition as a function of a magnetic field is generically accompanied by a metamagnetic transition [Fig. 1(a) and Ref. 33], the  $d\text{FSD}$  transition does not lead to a metamagnetic QCEP in the present model. It remains to be studied whether a concept of a metamagnetic QCEP can be a good basis to discuss electronic properties in  $\text{Sr}_3\text{Ru}_2\text{O}_7$  and how the putative QCEP can be related to the  $d\text{FSD}$  instability and the van Hove singularity. In this sense, it is important to clarify whether the anomalous  $T$  dependence of the resistivity observed around the metamagnetic transition[26] can be explained in terms of  $d\text{FSD}$  fluctuations and the van Hove singularity or whether we have to invoke quantum fluctuations originating from some QCEP.

Different scenarios from the  $d\text{FSD}$  and the QCEP were proposed for  $\text{Sr}_3\text{Ru}_2\text{O}_7$ , microscopic phase separation due to Coulomb energy[38] and magnetic domain formation due to long-range dipolar interactions.[39] In our analysis, we employ the ground canonical ensemble and a first order phase transition occurs as a function of a magnetic field or the chemical potential for low  $T$ . Such a transition in turn appears as a magnetic phase separation or an electronic phase separation as a function of its canonical conjugate variable, namely the magnetization [see Fig. 1(h)] or the electron density [see Fig. 1(g) in Ref. 10]. Therefore invoking the dipolar interaction or Coulomb force, we expect some inhomogeneous states in line with Refs. 38 and 39. However our possible inhomogeneous state may replace only phase separated regions in Fig. 1(h) and thus is realized only near a metamagnetic transition, in contrast to Refs. 38 and 39, where the inhomogeneous state is stabilized in the entire region of the phase diagram.



## VI. CONCLUSION

We have performed a comprehensive analysis of magnetic field effects on the  $d$ FSD instability in a one-band mean-field model with a pure forward scattering interaction. In the plane of  $\mu$  and  $h(> 0)$ , the  $d$ FSD instability occurs around the axis of  $\mu = \pm h$ , namely around the van Hove filling of the majority band ( $\mu < 0$ ) and the minority band ( $\mu > 0$ ), even in the limit of  $h \rightarrow \infty$ . The magnetic field, however, suppresses substantially the energy scale of the  $d$ FSD instability. The  $d$ FSD instability occurs through a second order transition at high  $T$  and typically changes to a first order transition at low  $T$ ; the end points of the second order line are tricritical points. Neither a QCP nor a QCEP of the  $d$ FSD is realized by the magnetic field in the present model. In the weak coupling limit, typical quantities characterizing the phase diagram have the field-independent single energy scale, while its dimensionless coefficient varies with the magnetic field. The magnetic field-induced  $d$ FSD instability is a promising scenario for  $\text{Sr}_3\text{Ru}_2\text{O}_7$  and we have discussed various future issues to establish such a scenario.

### Acknowledgments

The author is grateful to A. A. Katanin for collaboration on a related work and fruitful discussions. He also thanks C. Honerkamp, G. Khaliullin, A. P. Mackenzie, W. Metzner, and R. S. Perry for helpful discussions, and R. Zeyher for critical reading of the manuscript.

### APPENDIX A: PHASE DIAGRAM FOR $\mu = -0.35$ AND $-0.34$

Figures 1(a) and 2 are two typical phase diagrams as a function of  $h$  in the present model. These phase diagrams, however, are not connected smoothly by changing  $\mu$ . In fact, two other types of the phase diagram appear in a very limited  $\mu$  region as shown in Fig. 8. For  $\mu = -0.35$  [Fig. 8(a)], the dome-shaped transition line is realized on the relatively large  $h$  side. In addition, the region surrounded by a first order transition line appear around  $(h, T) = (0, 0)$ . At  $T = 0$ , therefore, there is reentrant behavior as a function of  $h$  and the symmetric phase appears in the intermediate  $h$  region ( $0.12 \lesssim h \lesssim 0.14$ ). For  $\mu = -0.34$  [Fig. 8(b)], the overall shape of the phase diagram is the same as that shown in Fig. 2, but a first order line appears for high  $T$  near  $h = 0$ , accompanied by a tricritical point. As a

result, a first order transition happens as a function of  $T$  in a sizable  $h$  region. This is a very special case in our model since a first order transition as a function of  $T$  is usually realized in a very limited  $h$  region as seen in Figs. 1(a) and 2.

These peculiar types of the phase diagrams are understood from Fig. 5(a) or similarly from Fig. 4(a). The first order transition line in Fig. 5(a) is almost straight near  $|\mu| \approx 1.3\epsilon_\Lambda e^{-1/(2\bar{g})}$  [ $\mu \approx -0.34$  in Fig. 4(b)]. Therefore we can have an extended  $h$  region of the first order transition as seen in Fig. 8(b). When we look at closely the region near  $|\mu| \approx 1.3\epsilon_\Lambda e^{-1/(2\bar{g})}$  and  $h \lesssim 0.54\epsilon_\Lambda e^{-1/(2\bar{g})}$  (inset of Fig. 5), the first order transition line turns out to have a small inward curvature. This is why a symmetric phase is intervened between the two  $d$ FSD phases in Fig. 8(a).

## APPENDIX B: SPIN-DEPENDENT $d$ -WAVE FERMI SURFACE DEFORMATION

We have analyzed the  $d$ -wave Fermi surface symmetry breaking in the charge channel. From the point of view of Landau Fermi liquids, we can consider Fermi surface instability also in the spin channel. This possibility was pursued in several references[45, 46, 47, 48] in the context of a general Landau Fermi liquid theory,[46, 47, 48] and a possible relation to a hidden order in URu<sub>2</sub>Si<sub>2</sub>. [45] Here we clarify the relation between the charge-channel  $d$ FSD and the spin-channel  $d$ FSD, and discuss its relevance to Sr<sub>3</sub>Ru<sub>2</sub>O<sub>7</sub>.

The minimal model for the spin-dependent  $d$ FSD reads

$$H = \sum_{\mathbf{k}, \sigma} (\epsilon_{\mathbf{k}}^0 - \mu) n_{\mathbf{k}\sigma} + \frac{1}{2N} \sum_{\mathbf{k}, \sigma, \mathbf{k}', \sigma'} f_{\mathbf{k}\mathbf{k}'}^a \mathbf{S}_{\mathbf{k}} \cdot \mathbf{S}_{\mathbf{k}'} - h \sum_{\mathbf{k}, \sigma} \sigma n_{\mathbf{k}\sigma}, \quad (\text{B1})$$

where  $\mathbf{S}_{\mathbf{k}} = \frac{1}{2} \sum_{\alpha, \beta} c_{\mathbf{k}\alpha}^\dagger \boldsymbol{\sigma}_{\alpha\beta} c_{\mathbf{k}\beta}$ ,  $f_{\mathbf{k}\mathbf{k}'}^a = -g^a d_{\mathbf{k}} d_{\mathbf{k}'}$ , and the rest of notation is the same as the model (1). Since the interaction has SU(2) symmetry and the magnetic field is assumed to be applied along the  $z$  direction, we assume that the  $S_z$  component can have a finite expectation value. Defining a mean field

$$\eta^a = -\frac{g^a}{N} \sum_{\mathbf{k}} d_{\mathbf{k}} \langle S_{\mathbf{k}}^z \rangle, \quad (\text{B2})$$

we obtain the mean-field Hamiltonian

$$H_{\text{MF}} = \sum_{\mathbf{k}, \sigma} \xi_{\mathbf{k}\sigma}^a n_{\mathbf{k}\sigma} + \frac{N}{2g^a} (\eta^a)^2 \quad (\text{B3})$$

where  $\xi_{\mathbf{k}\sigma}^a = \epsilon_{\mathbf{k}}^0 + \frac{1}{2}\sigma\eta^a d_{\mathbf{k}} - \mu_{\sigma}$ . The grand canonical potential per lattice site thus reads

$$\omega = -\frac{T}{N} \sum_{\mathbf{k},\sigma} \log(1 + e^{-\xi_{\mathbf{k}\sigma}^a/T}) + \frac{(\eta^a)^2}{2g^a} \quad (\text{B4})$$

$$= -\frac{T}{N} \sum_{\mathbf{k},\sigma} \log(1 + e^{-\xi_{\mathbf{k}\sigma}^{a'}/T}) + \frac{(\eta^a)^2}{2g^a}. \quad (\text{B5})$$

In the second line, we have introduced

$$\xi_{\mathbf{k}\sigma}^{a'} = \epsilon_{\mathbf{k}}^0 + \frac{1}{2}\eta^a d_{\mathbf{k}} - \mu_{\sigma}, \quad (\text{B6})$$

noting that  $d_{\mathbf{k}}$  changes its sign with respect to  $k_x \Leftrightarrow k_y$  so that  $\sigma d_{\mathbf{k}}$  in the original  $\xi_{\mathbf{k}\sigma}^a$  can be written as  $d_{\mathbf{k}}$  in Eq. (B6).

Comparing Eqs. (B5) and (B6) with Eqs. (7) and (6), respectively, we see that the free energy becomes exactly the same under the following mapping,

$$\frac{1}{2}\eta^a \Leftrightarrow \eta, \quad \frac{1}{4}g^a \Leftrightarrow g. \quad (\text{B7})$$

Hence the thermodynamics in the spin channel of the  $d$ FSD is the same as that in the charge channel in the sense that we obtain the exactly the same results as Figs. 1(a) and (e)-(h) under the mapping (B7). The difference appears in the ‘‘internal’’ structure of the order parameter and in a deformation of the FS. In the spin channel, we can write  $\frac{1}{2}\eta^a = \frac{1}{2} \sum_{\sigma} \sigma \eta_{\sigma}^a$ , where

$$\frac{1}{2}\eta_{\sigma}^a = -\frac{g^a}{4N} \sum_{\mathbf{k}} d_{\mathbf{k}} \langle n_{\mathbf{k}\sigma} \rangle \quad (\text{B8})$$

$$= \begin{cases} -\frac{g^a}{4N} \sum_{\mathbf{k}} d_{\mathbf{k}} f(\xi_{\mathbf{k}\uparrow}^{a'}) & \text{for } \sigma = \uparrow \\ +\frac{g^a}{4N} \sum_{\mathbf{k}} d_{\mathbf{k}} f(\xi_{\mathbf{k}\downarrow}^{a'}) & \text{for } \sigma = \downarrow. \end{cases} \quad (\text{B9})$$

Comparing with Eq. (9), we see the relation under the mapping (B7)

$$\frac{1}{2}\eta_{\uparrow}^a \Leftrightarrow \eta_{\uparrow}, \quad -\frac{1}{2}\eta_{\downarrow}^a \Leftrightarrow \eta_{\downarrow}. \quad (\text{B10})$$

As we have actually seen in the numerical result in Sec. III,  $\eta_{\uparrow}$  in general has the same sign as  $\eta_{\downarrow}$  in the charge channel. Therefore  $\eta_{\uparrow}^a$  has an opposite sign of  $\eta_{\downarrow}^a$  as seen in Fig. 9(a). While we have introduced  $\xi_{\mathbf{k}\sigma}^{a'}$  [Eq. (B6)], the Fermi surface itself is defined by  $\xi_{\mathbf{k}\sigma}^a = 0$ . Since  $\xi_{\mathbf{k}\sigma}^a$  contains a factor  $\sigma\eta^a d_{\mathbf{k}}$ , a Fermi surface deformation in the spin channel occurs always in the opposite direction between the up-spin and the down-spin electron band as

shown in Fig. 9(b); note that the deformation is determined by  $\eta^a$ , not by  $\eta_\sigma^a$ . As a result, the net deformation of the band is partially compensated. This is a crucial difference from the  $d$ FSD instability in the charge channel.

The recent experiment by Borzi *et al.*[32] showed a strong  $xy$ -anisotropy of the magnetoresistivity by applying an additional small magnetic field to the  $\text{RuO}_2$  plane. This strong anisotropy may be discussed more naturally in terms of the  $d$ FSD instability in the charge channel rather than the spin channel. A conclusive discussion on which channel is more dominant would be to study microscopic deviation of the  $d$ FSD attractive interaction in both charge and spin channel in the context of  $\text{Sr}_3\text{Ru}_2\text{O}_7$  and to compare the strength of the each channel.

- 
- [1] H. Yamase and H. Kohno, *J. Phys. Soc. Jpn.* **69**, 332 (2000); **69**, 2151 (2000).
- [2] A. Miyanaga and H. Yamase, *Phys. Rev. B* **73**, 174513 (2006).
- [3] B. Edegger, V. N. Muthukumar, and C. Gros, *Phys. Rev. B* **74**, 165109 (2006).
- [4] C. J. Halboth and W. Metzner, *Phys. Rev. Lett.* **85**, 5162 (2000).
- [5] I. Grote, E. K rding, and F. Wegner, *J. Low Temp. Phys.* **126**, 1385 (2002); V. Hankevych, I. Grote, and F. Wegner, *Phys. Rev. B* **66**, 094516 (2002).
- [6] A. Neumayr and W. Metzner, *Phys. Rev. B* **67**, 035112 (2003).
- [7] B. Valenzuela and M. A. H. Vozmediano, *Phys. Rev. B* **63**, 153103 (2001).
- [8] I. J. Pomeranchuk, *Sov. Phys. JETP* **8**, 361 (1958).
- [9] I. Khavkine, C.-H. Chung, V. Oganessian, and H.-Y. Kee, *Phys. Rev. B* **70**, 155110 (2004).
- [10] H. Yamase, V. Oganessian, and W. Metzner, *Phys. Rev. B* **72**, 35114 (2005).
- [11] C. Honerkamp, M. Salmhofer, and T. M. Rice, *Eur. Phys. J. B* **27**, 127 (2002).
- [12] A. P. Kampf and A. A. Katanin, *Phys. Rev. B* **67**, 125104 (2003).
- [13] H. Yamase, *Phys. Rev. Lett.* **93**, 266404 (2004).
- [14] V. Hinkov, S. Pailh s, P. Bourges, Y. Sidis, A. Ivanov, A. Kulakov, C. T. Lin, D. Chen, C. Bernhard, and B. Keimer, *Nature (London)* **430**, 650 (2004).
- [15] H. Yamase and W. Metzner, *Phys. Rev. B* **73**, 214517 (2006).
- [16] S. A. Kivelson, E. Fradkin, and V. J. Emery, *Nature (London)* **393**, 550 (1998).
- [17] S. A. Grigera, P. Gegenwart, R. A. Borzi, F. Weickert, A. J. Schofield, R. S. Perry, T. Tayama, T. Sakakibara, Y. Maeno, A. G. Green, and A. P. Mackenzie, *Science* **306**, 1154 (2004).
- [18] A. P. Mackenzie and Y. Maeno, *Rev. Mod. Phys.* **75**, 657 (2003).
- [19] Q. Huang, J. W. Lynn, R. W. Erwin, J. Jarupatrakorn, and R. J. Cava, *Phys. Rev. B* **58**, 8515 (1998).
- [20] S.-I. Ikeda, Y. Maeno, S. Nakatsuji, M. Kosaka, and Y. Uwatoko, *Phys. Rev. B* **62**, R6089 (2000).
- [21] S.-I. Ikeda, N. Shirakawa, T. Yanagisawa, Y. Yoshida, S. Koikegami, S. Koike, M. Kosaka, and Y. Uwatoko, *J. Phys. Soc. Jpn.* **73**, 1322 (2004).
- [22] L. Capogna, E. M. Forgan, S. M. Hayden, A. Wildes, J. A. Duffy, A. P. Mackenzie, R. S. Perry, S. Ikeda, Y. Maeno, and S. P. Brown, *Phys. Rev. B* **67**, 012504 (2003).

- [23] I. Hase and Y. Nishihara, *J. Phys. Soc. Jpn.* **66**, 3517 (1997).
- [24] D. J. Singh and I. I. Mazin, *Phys. Rev. B* **63**, 165101 (2001).
- [25] S. A. Grigera, R. S. Perry, A. J. Schofield, M. Chiao, S. R. Julian, G. G. Lonzarich, S. I. Ikeda, Y. Maeno, A. J. Millis, and A. P. Mackenzie, *Science* **294**, 329 (2001).
- [26] R. S. Perry, L. M. Galvin, S. A. Grigera, L. Capogna, A. J. Schofield, A. P. Mackenzie, M. Chiao, S. R. Julian, S. I. Ikeda, S. Nakatsuji, Y. Maeno, and C. Pfleiderer, *Phys. Rev. Lett.* **86**, 2661 (2001).
- [27] Z. X. Zhou, S. McCall, C. S. Alexander, J. E. Crow, P. Schlottmann, A. Bianchi, C. Capan, R. Movshovich, K. H. Kim, M. Jaime, N. Harrison, M. K. Hass, R. J. Cava, and G. Cao, *Phys. Rev. B* **69**, 140409(R) (2004).
- [28] R. S. Perry, T. Tayama, K. Kitagawa, T. Sakakibara, K. Ishida, and Y. Maeno, *J. Phys. Soc. Jpn.* **74**, 1270 (2005).
- [29] P. Gegenwart, F. Weickert, M. Garst, R. S. Perry, and Y. Maeno, *Phys. Rev. Lett.* **96**, 136402 (2006).
- [30] K. Kitagawa, K. Ishida, R. S. Perry, T. Tayama, T. Sakakibara, and Y. Maeno, *Phys. Rev. Lett.* **95**, 127001 (2005).
- [31] S. A. Grigera, A. P. Mackenzie, A. J. Schofield, S. R. Julian, and G. G. Lonzarich, *Int. J. Mod. Phys. B* **16**, 3258 (2002).
- [32] R. A. Borzi, S. A. Grigera, J. Farrell, R. S. Perry, S. J. S. Lister, S. L. Lee, D. A. Tennant, Y. Maeno, and A. P. Mackenzie, *Science* **315**, 214 (2007).
- [33] H.-Y. Kee and Y. B. Kim, *Phys. Rev. B* **71**, 184402 (2005).
- [34] H. Yamase and A. A. Katanin, *cond-mat/0701628*.
- [35] B. Binz and M. Sigrist, *Europhys. Lett.* **65**, 816 (2004).
- [36] D. Belitz, T. R. Kirkpatrick, and J. Rollbühler, *Phys. Rev. Lett.* **94**, 247205 (2005).
- [37] A. J. Millis, A. J. Schofield, G. G. Lonzarich, and S. A. Grigera, *Phys. Rev. Lett.* **88**, 217204 (2002).
- [38] C. Honerkamp, *Phys. Rev. B* **72**, 115103 (2005).
- [39] B. Binz, H. B. Braun, T. M. Rice, and M. Sigrist, *Phys. Rev. Lett.* **96**, 196406 (2006).
- [40] A. G. Green, S. A. Grigera, R. A. Borzi, A. P. Mackenzie, R. S. Perry, and B. D. Simons, *Phys. Rev. Lett.* **95**, 86402 (2005).
- [41] The  $d$ FSD tendency in the  $t$ - $J$  model is observed in a rather wide doping region.[1, 3].

- [42] N. Kikugawa, C. Bergemann, A. P. Mackenzie, and Y. Maeno, Phys. Rev. B **70**, 134520 (2004).
- [43] H. Yamase and W. Metzner, Phys. Rev. B **75**, 155117 (2007).
- [44] S. A. Grigera, R. A. Borzi, A. P. Mackenzie, S. R. Julian, R. S. Perry, and Y. Maeno, Phys. Rev. B **67**, 214427 (2003).
- [45] C. M. Varma and L. Zhu, Phys. Rev. Lett. **96**, 036405 (2006).
- [46] J. Quintanilla and A. J. Schofield, Phys. Rev. B **74**, 115126 (2006).
- [47] P. Wölfle and A. Rosch, cond-mat/0609343.
- [48] C. Wu, K. Sun, E. Fradkin, and S.-C. Zhang, Phys. Rev. B **75**, 115103 (2007).

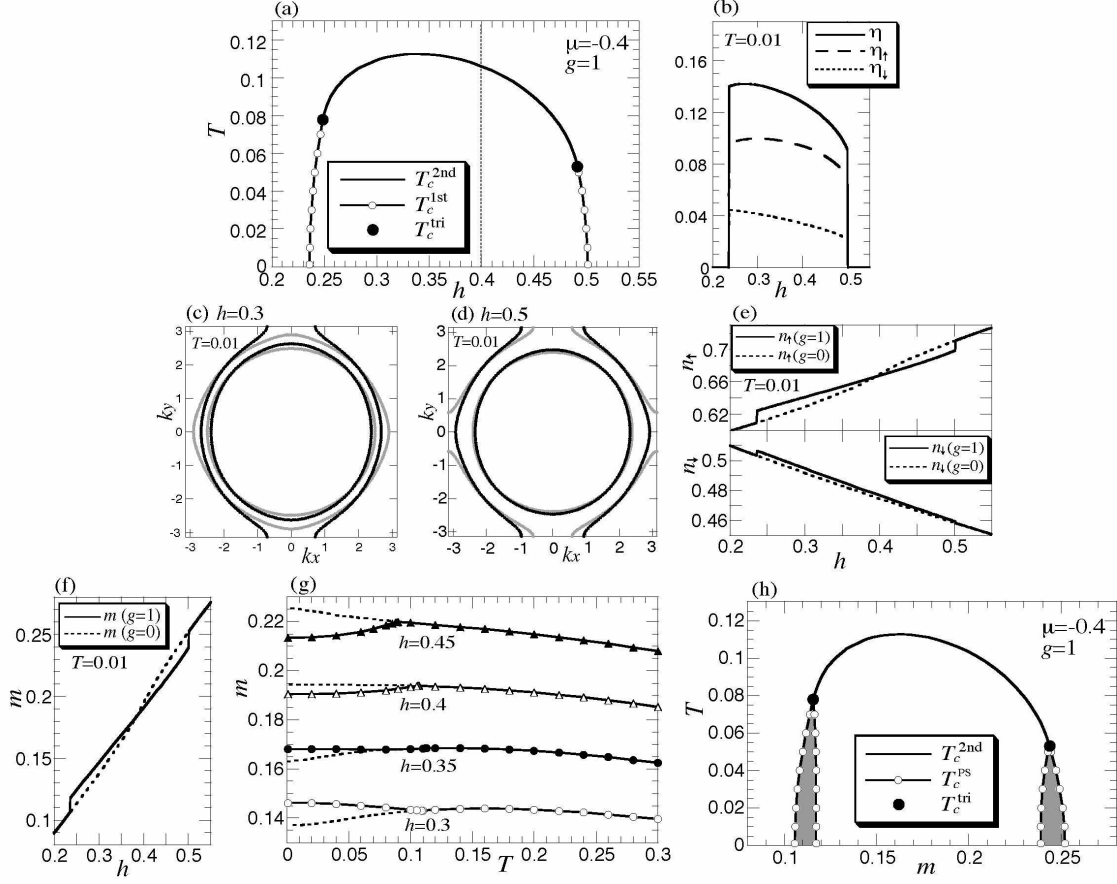


FIG. 1: The mean-field solution for  $t'/t = 0.35$ ,  $g = 1$ , and  $\mu = -0.4$ . (a)  $h$ - $T$  phase diagram; the transition line contains a second order line,  $T_c^{2nd}$ , for high  $T$  and two first order line,  $T_c^{1st}$ , for low  $T$ ; the solid circles are tricritical points; the dotted line denotes the van Hove energy of the up-spin band. (b)  $h$  dependence of the order parameter at  $T = 0.01$ ; note that  $\eta = \eta_{\uparrow} + \eta_{\downarrow}$ . (c) and (d) FSs for  $h = 0.3$  and  $0.5$  at  $T = 0.01$ ; the solid lines (gray lines) are FSs for  $g = 1$  ( $g = 0$ ); the deformation of the inner FS in (d) is hardly visible. (e)  $h$  dependence of  $n_{\sigma}$  at  $T = 0.01$  for  $g = 1$  (solid line) and  $0$  (dotted line). (f)  $h$  dependence of the magnetization at  $T = 0.01$  for  $g = 1$  (solid line) and  $0$  (dotted line). (g)  $T$  dependence of the magnetization for several choices of  $h$ ; the dotted line represents the result for  $g = 0$ . (h)  $m$ - $T$  phase diagram; the system undergoes phase separation in the shaded regions surrounded by  $T_c^{PS}$ ; the other notation is the same as that in (a).



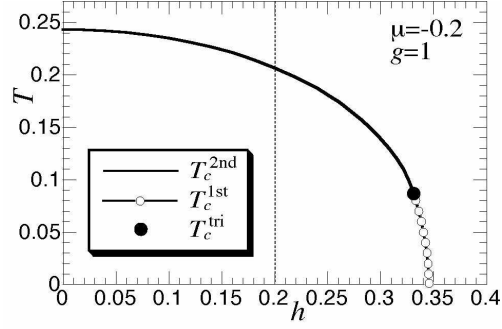


FIG. 2:  $h$ - $T$  phase diagram for  $t'/t = 0.35$ ,  $g = 1$ , and  $\mu = -0.2$ ; the notation is the same as that in Fig. 1(a).

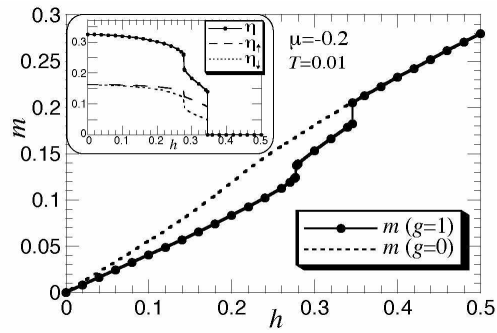


FIG. 3:  $h$  dependence of  $m$  at  $\mu = -0.2$  and  $T = 0.01$  for  $g = 1$  (solid line) and  $0$  (dotted line). The inset shows the  $h$  dependence of the order parameter.

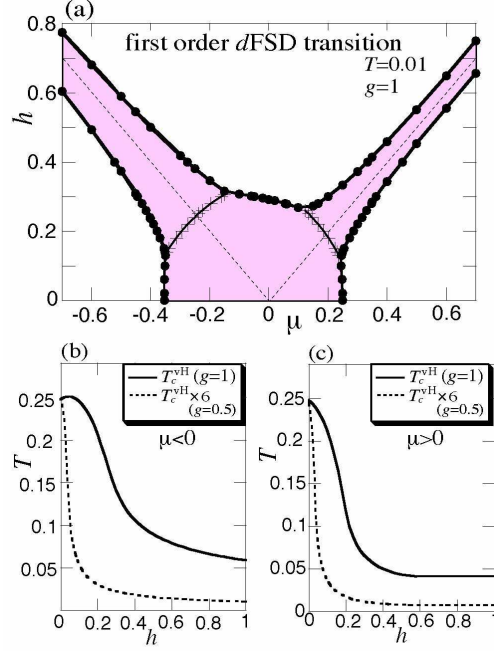


FIG. 4: (Color online) (a) The first order  $d$ FSD transition line in the plane of  $\mu$  and  $h$  at  $T = 0.01$  for  $g = 1$ ; the symmetry-broken phase is stabilized in the colored (shaded) area; for notation, see the text. (b) and (c)  $h$  dependence of  $T_c$  along the van Hove energy, namely along the dotted line in (a) for  $\mu < 0$  and  $\mu > 0$ , respectively; the solid (dotted) line is the result for  $g = 1$  (0.5);  $T_c^{\text{vH}}$  for  $g = 0.5$  is multiplied by 6.

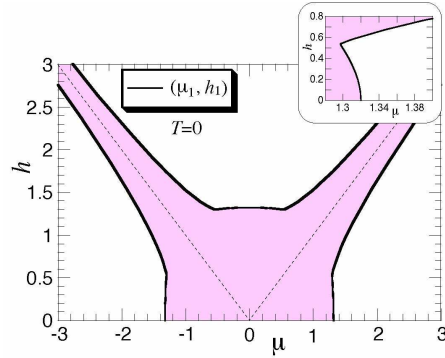


FIG. 5: (Color online) The first order  $d$ FSD transition line in the weak coupling limit in the plane of  $\mu$  and  $h$  at  $T = 0$ ;  $\mu$  and  $h$  are scaled by the energy  $\epsilon_{\Lambda} e^{-1/(2g)}$ ; the symmetry-broken phase is stabilized in the colored (shaded) area; the dotted line represents the van Hove energy of the up-spin band ( $\mu < 0$ ) and the down-spin band ( $\mu > 0$ ). The inset magnifies the region around  $\mu \approx 1.3$ .

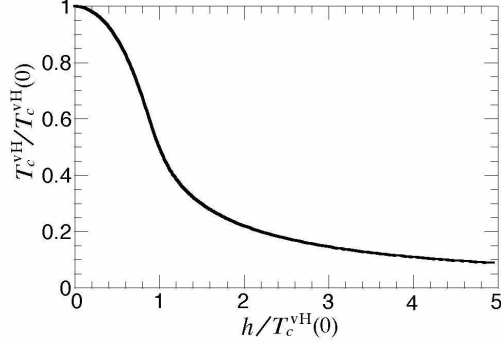


FIG. 6:  $T_c$  along the van Hove energy, namely along the line of  $h = |\mu|$ , in the weak coupling limit;  $T_c$  and  $h$  are scaled by  $T_c^{\text{vH}}(0)$ .

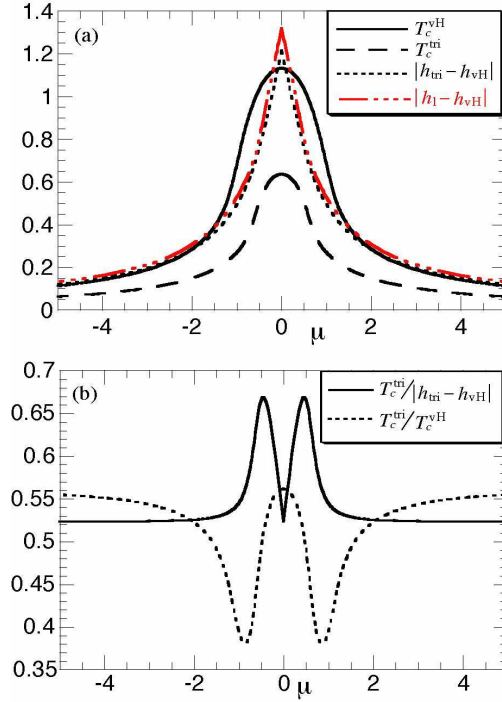


FIG. 7: (Color online) (a)  $\mu$  dependence of  $T_c^{\text{vH}}$ ,  $T_c^{\text{tri}}$ ,  $h_{\text{tri}} - h_{\text{vH}}$ , and  $h_1 - h_{\text{vH}}$ , where  $h_{\text{vH}} = |\mu|$ ; all quantities are scaled by the energy  $\epsilon_\Lambda e^{-1/(2\bar{g})}$ . (b)  $\mu$  dependence of the universal ratios  $T_c^{\text{tri}}/|h_{\text{tri}} - h_{\text{vH}}|$  and  $T_c^{\text{tri}}/T_c^{\text{vH}}$ .

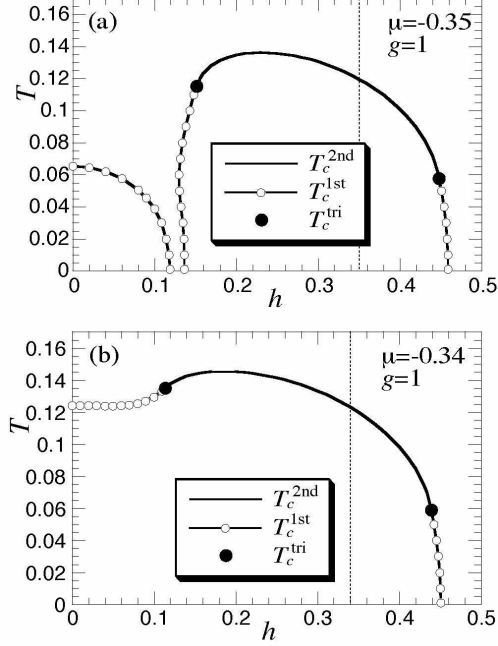


FIG. 8:  $h$ - $T$  phase diagram for  $\mu = -0.35$  (a) and  $\mu = -0.34$  (b) for  $t'/t = 0.35$  and  $g = 1$ ; the notation is the same as that in Fig. 1(a).

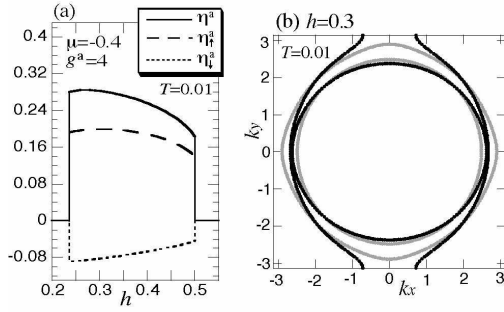


FIG. 9: The mean-field solution in the spin-channel  $d$ FSD instability for  $t'/t = 0.35$ ,  $\mu = -0.4$ , and  $g^a = 4$ . (a)  $h$  dependence of the order parameter at  $T = 0.01$ . (b) FSs at  $h = 0.3$  (solid lines); the gray lines denote the FSs for  $g^a = 0$ .